

Determination of resonance locations in barred spiral galaxies using multiband photometry

Amber D. Sierra^{1,2*}, Marc S. Seigar^{1,3†}, Patrick Treuthardt⁴, and Ivânio Puerari⁵

¹*Department of Physics & Astronomy, University of Arkansas at Little Rock, 2801 S. University Avenue, Little Rock, AR 72204-1099, USA*

²*Department of Physical Sciences, Arkansas Tech University, 1701 N. Boulder Ave, Russellville, AR 72801, USA*

³*Department of Physics, University of Minnesota Duluth, 1023 University Drive, Duluth, MN 55812-3009, USA*

⁴*Astronomy & Astrophysics Research Laboratory, North Carolina Museum of Natural Sciences, 11 W. Jones Street, Raleigh, NC 27601, USA*

⁵*Instituto Nacional de Astrofísica, Óptica y Electrónica, Apdo. Postal 51 y 216, 72000 Puebla, Puebla, Mexico*

ABSTRACT

In this paper, we apply a method identified by Puerari & Dottori to find the corotation radii (CR) in spiral galaxies. We apply our method to 57 galaxies, 17 of which have already have their CR locations determined using other methods. The method we adopted entails taking Fourier transforms along radial cuts in the u , g , r , i , and z wavebands and comparing the phase angles as a function of radius between them. The radius at which the phase angles cross indicates the location of the corotation radius. We then calculated the relative bar pattern speed, \mathcal{R} , and classified the bar as “fast”, where $\mathcal{R} < 1.4$, slow, where $\mathcal{R} \geq 1.4$, or intermediate, where the errors on \mathcal{R} are consistent with the bar being “slow” or “fast”. For the 17 galaxies that had their CR locations previously measured, we found that our results were consistent with the values of \mathcal{R} obtained by the computer simulations of Rautiainen, Salo & Laurikainen. For the larger sample, our results indicate that 34 out of 57 galaxies ($\simeq 60\%$) have fast bars. We discuss these results in the context of its implications for dark matter concentrations in disk galaxies. We also discuss these results in the context of different models for spiral structure in disk galaxies.

Key words: galaxies: spiral – galaxies: structure

1 INTRODUCTION

The presence and location of corotation resonances in barred spiral galaxies is important for several reasons. First, resonances are required by density wave theory, so their existence would be evidence that supports the theory. Second, the corotation resonance of a bar is related to the ability to transfer angular momentum outwards, or material inwards. This is the main process that drives the secular evolution of a galaxy. Also, resonances can scatter stellar orbits and cause disk heating. Finally, the corotation radius of barred galaxies is related to the bar pattern speed. Fast bars may indicate low concentration central dark matter halos due to decreased dynamical friction (Debatista & Sellwood 2000).

Current methods of measuring corotation resonance (CR) radii and/or bar pattern speeds, e.g., computer simulations (Rautiainen et al. 2008; Treuthardt et al. 2012), the Tremaine-Weinberg method (Tremaine & Weinberg 1984;

hereafter TW), etc., require extensive computer and telescope time, the presence of specific morphological features, or other limiting factors. The TW method directly measures the bar pattern speed, but it requires a lot of telescope time. Also, it is only useful on galaxies where the bar major axis and galaxy major axis are offset by 45° , or as close to 45° as possible. This severely limits the number of galaxies you can analyze with the TW method. Therefore, other methods have been found to estimate the bar pattern speed, such as the dimensionless parameter \mathcal{R} , which estimates the relative bar pattern speed. \mathcal{R} is defined as the bar corotation radius divided by the bar radius, $\mathcal{R} = R_{\text{CR}}/R_{\text{bar}}$. When finding the relative bar pattern speed, the focus is on determining the radius of the bar’s corotation resonance. Rather than make use of TW, it would be beneficial to have a faster, cheaper, but reliable method for determining corotation resonance radii and relative bar pattern speeds. Puerari & Dottori (1997; hereafter PD) present such a method. In this study, we use the PD method to measure the CR radii and relative bar pattern speed of 15 barred spiral galaxies that already have CR measurements elsewhere in the literature.

* E-mail: asierra1@atu.edu

† E-mail: msseigar@d.umn.edu

Resonances are predicted by density wave theory, which was originally proposed by Lin & Shu (1964). Further developments of the theory have led to the modal theory of spiral structure (e.g., Bertin et al. 1989a, b; Bertin 1993; Bertin & Lin 1996). In these models, the spiral density wave has a pattern speed which is independent of the orbital speeds of stars and gas in the disk. If the relative velocities between the gas and the density wave are supersonic, a shock front may be formed (Roberts 1969; Binney & Tremaine 2008). The shock compresses the gas, which after a time delay leads to star formation on the side of the arm opposite the shock front (Seigar & James 2002).

When observed in the near-infrared, about two-thirds of all disk galaxies seem to have a bar-like structure with their own pattern speeds (Seigar et al. 1998; Eskridge et al. 2000; Hernandez et al. 2005). In barred-spiral galaxies, the bar forcing influences the spiral arm amplitudes. Specifically, Salo et al. (2010) found a strong correlation between the local tangential bar torque, $Q_{\text{bar}}(r)$, and the local spiral arm amplitude, $A_2(r)$, out to 1.5 bar lengths. This suggests that the inner portions of spiral arms may be either a continuation of the bar mode or they are driven by bar forcing itself. Further out, the spirals are most likely independent modes, and the disk pattern speed becomes the dominant factor. The radius where the angular velocity of the stars is equal to a pattern speed is called a corotation radius. According to Contopoulos (1980), the radius of the bar cannot be larger than its corotation radius, or the bar would not be self-sustaining (i.e., it simply would not exist). Note that Buta & Zhang (2009) find some bars that are larger than their CR radii, but this is considered controversial.

Beckman & Cepa (1990) showed that azimuthal color profiles of galaxies can be a useful tool in studying spiral galaxies. Phase shifts in the profiles of the B and I band can highlight star-forming regions in galaxies. PD expanded on the findings of Beckman & Cepa (1990) by showing that phase crossings of the B and I bands indicate a corotation radius. The motion of the spiral density wave creates a shock front inducing star formation. Because new stars are bluer than older stars, the side of the spiral arm with the shock front should be bluer. Inside corotation the material speed is greater than the bar pattern speed. This means that the inner edge of the spiral pattern is bluer than the outer edge. This is because gas clouds enter the density wave and create a shock front as they enter. Bright, blue, newly formed stars then appear downstream of this shock. Outside corotation the bar pattern speed is faster and the color of the two sides switch. At corotation the bar pattern speed and material speed are equal. At this radius the shock wave switches sides. We refer the reader to PD (their Figure 1) to see how the shock front would switch sides at the CR.

PD describes the photometric method for determining corotation radius and included two example galaxies, NGC 7479 and NGC 1832. Aguerri, Beckman & Prieto (1998) reported the CR, determined by using the PD method, for 10 galaxies. During the next decade, references were made to the PD method (e.g., Aguerri et al. 2000; Rautiainen, Salo & Laurikainen 2008) but its usage was absent from the literature. Martínez-García et al. (2009a) reported their results on the relationship between color gradients and pattern speed. They found that 10 out of the 13 barred and non-barred spiral galaxies in their sample showed color gradients that

matched the theoretical predictions. Martínez-García et al. (2009b) describe the effect non-circular motions have on the azimuthal color gradient. The initial assumptions for the formation of a color gradient involved the collision of a spiral density wave and the disc material, whose orbital velocities decrease with radial distance. Martínez-García et al. (2009b) showed that legitimate color gradients could form in galaxies even if the disc material moved in non-circular orbits.

Finally, Martínez-García & Puerari (2014) reported results using the PD method on 9 nearby spiral galaxies. Instead of using optical wavebands, they used HI, CO, 24- μm , and FUV wavebands. They were able to find phase shifts. As noted in previous work by Martínez-García et al. (2009a), color gradients are common in spiral arms. Although the gradients do not always occur across a large enough radial range to be sufficient for finding resonance locations, Martínez-García & González-Lópezlira (2013) found that at least 50% of their studied objects did have a sizeable region of color gradients in the spiral arms. Martínez-García & Puerari (2014) showed that the phase shifts discovered in two arm spirals are different for the two arms. However, they were looking for the spiral arm pattern speed. In this paper, we focus on the bar pattern speed, which occurs very near the end of the bar which is more symmetrical in nature.

An alternative theory of spiral structure, particularly in barred galaxies, is referred to as manifold theory (Romero-Gómez et al. 2006; Romero-Gómez et al. 2007, Athanassoula et al. 2009a, b; Athanassoula et al. 2010). These authors studied the orbits of individual particles. Athanassoula summarizes one of the differences between manifold and spiral density wave theory as: “In density wave theory, the arms are loci of density maxima. Particles should thus traverse the arms, but stay longer in the arm than in the interarm region (Lin & Shu 1964). This is totally different from our manifold theory, where spiral arms should be a bundle of orbits guided by the manifolds, so that particles should move along the arms rather than across them” (Athanassoula 2012).

If the stars or particles travel along the arms instead of across them, then any age gradients or color gradients should also be along the arms instead of across them. Therefore, if we could show many examples of age gradients across spiral arms, this would favor density wave theory over manifold theory.

As well as the PD method, multiple methods for finding the R_{CR} have been developed. A few example methods are listed below.

- Morphological, e.g., rings (Patsis et al. 2003): The rings of galaxies can be related to resonances locations. The nuclear, inner, and outer rings can be linked to the inner Lindblad resonance, inner ultraharmonic resonances, and outer Lindblad resonances.
- Computer modeling, e.g., Sticky-Particle (Rautiainen et al. 2008; Treuthardt et al. 2012) or hydrodynamics (Lin, Yuan & Buta 2008): Virtual particles are used to simulate the response of gas clouds in a gravitational potential.
- Phase shift between potential and density (Zhang & Buta 2007): A method for determining the corotation radii and pattern speed of galactic density waves using the azimuthal phase shift between the potential and density wave patterns.

In this paper, we use the results of our PD analysis and

compare them to the latter two methods described above. We do not make any comparisons with the first method, since the method has large uncertainties.

This paper is organized as follows: Section 2 describes the dataset and methods used; Section 3 presents the corotation radii that we have determined; Section 4 presents and discusses our results; and in Section 5 we summarize our main conclusions.

2 DATA AND METHODS

2.1 Sample Description

One of the major benefits of using the PD method for finding bar corotation radii (and then the relative bar pattern speed) is that existing images can be used. The sample of galaxies we used in this study was drawn from the EFIGI (Extraction de Formes Idealises de Galaxies en Imagerie) survey (Baillard et al. 2011). EFIGI consists of 4458 galaxies from the Third Reference Catalogue of Bright Galaxies (de Vaucouleurs et al. 1991; hereafter RC3). The u , g , r , i , and z -band images for these galaxies are taken from the Sloan Digital Sky Survey (SDSS) Data Release 4 (DR4; Adelman-McCarthy et al. 2006). Each of the images is 255×255 pixels and scaled so that the D_{25} isophote of each galaxy (taken from RC3) fits into the center 169×169 pixels. The angular pixel scale is then increased by 33%. While it is helpful that all of the images are the same size (255×255 pixels), the pixel scale for all of the images is different and must be calculated for each galaxy. In order to do this, the D_{25} values in arcseconds from the RC3 for each galaxy were taken from the NASA/IPAC Extragalactic Database (NED)¹. Using this, we then determined the pixel scale for each image.

The EFIGI Hubble Sequence (EHS) and the Hubble classification from RC3 are very similar. The two are identical for the main galaxy sequence (Baillard et al. 2011). EHS types are categorized by the numbers -6 to 11, with spiral galaxies having the values 0 to 9 (see Baillard et al. 2011, their Table 1). Barred and non-barred spiral galaxies do not have separate classifications in EHS, but various attributes of the galaxies are categorized, including bar length (see Table 1 for a list of attributes). Each attribute was rated 0, 0.25, 0.5, 0.75, or 1 based upon the strength of their presence in the galaxy.

We arrived at our sample of 57 galaxies by searching the EFIGI catalogue for suitable galaxies to which the PD method could be applied. A list of galaxies with the following attributes were identified: (1) Hubble types Sab through Scd, (2) bar length $0.25D_{25} \leq R_{\text{bar}} \leq 1.00D_{25}$, and (3) inclination angle $i < 60^\circ$. A total of 100 galaxies fit these criteria. However, we could only successfully apply the PD method to 57 of them (for reasons discussed in section 3).

Within our final sample of 57 galaxies, 10 had relative bar pattern speeds measured through sticky particle simulations by Rautiainen et al. (2008). After the methodology was applied to the original sample of 10 galaxies, a second

comparison set of galaxies was chosen. Buta & Zhang (2009) used a method comparing the gravitational potential and the spiral density wave to find the corotation radius. Then they used their results to determine relative bar pattern speeds for 101 galaxies. The Buta & Zhang galaxies included the 10 galaxies from the original comparison sample plus an additional 7 galaxies for which we could find CR locations using the EFIGI data.

2.2 Mask Creation

Galaxy images can contain foreground objects (such as stars) or other, background galaxies. These extra objects need to be isolated and removed from the image, so that only the galaxy of interest is being analyzed. The program Source Extractor (Bertin & Arnouts 1996) was used to find the location of foreground and background objects. Using these locations, we then used IRAF to create a mask for each galaxy image.

2.3 Image Deprojection

The galaxies were deprojected by fitting elliptical isophotes to the galaxy image with the IRAF task `ellipse`. The ellipticity of the outer isophotes describes how far the galaxy is from being face on, or in other words, the inclination of the galaxy. For a face-on or deprojected galaxy, the outer isophotes of the galaxy are assumed to be intrinsically circular. Deprojection of the galaxy images was performed by rotating the images through an angle equal to the position angle of the major-axis determined using `ellipse`. The images were then stretched in the x -direction by an amount determined from their ellipticity. Finally, each image was viewed to verify that the outer isophote appears approximately circular.

It is important to make sure that all of the bands of a galaxy are identically deprojected. For this study, a combined image was created by adding the u , g , r , i , and z -band images together. This combined image was then deprojected and the position angle and ellipticity for it was applied to each individual waveband image.

2.4 Determination of Bar Radius

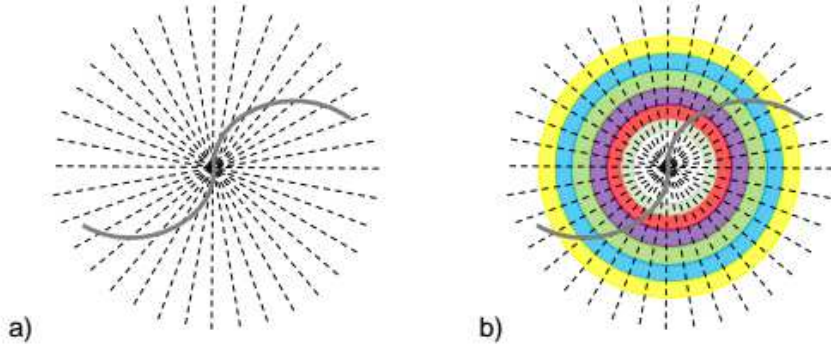
The deprojected galaxy was viewed in the i -band and the approximate visual end of the bar was recorded. Then the IRAF task `ellipse`, along with the methodology described in Wozniak et al. (1995), was used to find the end of the bar. The position angle (PA) and ellipticity were plotted against the square root of the radius to identify better detail in the inner regions of the image. Wozniak et al. (1995) also described how these plots could show structure in the bar (see their Figure 1). For instance, in a plot of ellipticity as a function of radius (or \sqrt{r}), a bar shows up as having a high ellipticity, and at the end of the bar there is a sudden change back to the minimum ellipticity, e_{min} . Similarly, the PA changes abruptly at the end of the bar.

In this study, the point where the PA is no longer constant did not always line up with the return of the ellipticity to e_{min} . In those cases, the radius at which the PA began to change (the end of the flat region) was taken to be the end

¹ The NASA/IPAC Extragalactic Database (NED) is operated by the Jet Propulsion Laboratory, California Institute of Technology, under contract with the National Aeronautics and Space Administration.

Table 1. EFIGI galaxy attributes according to their six classifications as labelled in the column headings.

Appearance	Environment	Bulge	Spiral Arm Properties	Textural Appearance	Dynamical Features
Inclination/ elongation	Multiplicity	B/T ratio	Arm strength	Visible dust	Bar length
	Contamination		Arm curvature	Dust dispersion	Inner ring
			Rotation	Flocculence	Outer ring
				Hot spots	Pseudo-ring
					Perturbation

**Figure 1.** (a) Galaxy images divided into azimuthal sections and (b) galaxy images divided azimuthally and radially.

of the bar. Additionally discontinuities in the PA vs. \sqrt{r} and ellipticity vs. \sqrt{r} near the visual end of the bar were chosen as the end of the bar.

2.5 Fourier Transformations of Galaxy Images

We use a code that creates azimuthal profiles of the galaxies and then performs Fourier transforms on them. The first step of the code is to divide the image into a chosen number of azimuthal and radial sections (see Figure 1). We set up the code with 180 azimuthal sections, each 2° wide, and 120 radial sections, each 1 pixel wide. Each galaxy was analyzed from a radius of 4 pixels to a radius of 124 pixels. An azimuthal profile was created at each radial division. The code was then run to determine the Fourier transforms of the azimuthal profiles,

$$F_2(r) = \int_{-\pi}^{\pi} I_r(\theta) e^{-2i\theta} d\theta \quad (1)$$

where the associated phase angles are given by

$$\theta(r) = \tan^{-1} \frac{\text{Re}[F_2(r)]}{\text{Im}[F_2(r)]} \quad (2)$$

where $\text{Re}[F_2(r)]$ and $\text{Im}[F_2(r)]$ are the real and imaginary parts of the complex Fourier coefficient, $F_2(r)$. The phase angle as a function of radius for each waveband was then plotted on the same graph. Locations where the waveband phase angles intersect are indicative of corotation radii.

2.6 Determination of Corotation Radii

The phase angle of the u , g , r , i , and z -bands versus the radius was plotted. The radii where the phase angles cross were then identified. The initial identification occurred by calculating the phase difference, $\theta_g - \theta_z$, at each radius and interpolating between consecutive radii. Then all radii for which the phase difference equals zero are recorded. The first phase crossing following the end of the bar is the one associated with the corotation radius of the bar. For all 5 wavebands, there are 10 pairs – ug , ur , ui , uz , gr , gi , gz , ri , rz , and iz . The values of $R_{\text{CR,min}}$ and $R_{\text{CR,max}}$ were found for each of the 10 pairs. The lowest $R_{\text{CR,min}}$ and the greatest $R_{\text{CR,max}}$ were used as the range for calculating the average phase crossing. Any crossings that occurred in that range were included in the average and then a standard deviation of those values was calculated. This is then reported as the bar corotation radius

The likelihood of confusion with the corotation radius due to the spiral arm pattern speed is significantly minimized due to the relationship between the local tangential bar forcing, $Q_{\text{bar}}(r)$, and the local spiral amplitude, $A_2(r)$, reported by Salo et al. (2010). This relationship was found to be satisfied out to a radius $r \sim 1.5R_{\text{bar}}$. Within this region it is likely that the stellar spirals are either a continuation of the bar mode or they are driven by the bar. This relationship, as found by Salo et al. (2010), gives an estimate of the extent of bar-driving. It therefore seems that in the regions where we are finding the corotation radii (the loca-

Table 2. Bar, CR radii, and relative bar pattern speeds for the entire sample of 57 galaxies. Columns 1 and 2 list the galaxy names from the PGC and NGC catalogues; Column 3 lists the Hubble types from the RC3; Column 4 lists the D_{25} in arcsec; Column 5 lists the pixel scale; Columns 6 and 7 lists the corotation radius in pixels and arcseconds respectively; Columns 8 and 9 list the bar radius; Column 10 lists the relative bar pattern speed; Column 11 lists the relative bar pattern speed determined by Rautiainen et al. (2008) using Sticky Particle Simulations where available; Column 12 gives the percentage difference between the relative bar pattern speeds listed in Columns 10 and 11; and Column 13 gives the bar pattern speed as determined from the potential-density phase-shift method (Buta & Zhang 2009). Note that for three galaxies the value for D_{25} was not available in the RC3, and therefore it was not possible to determine a pixel scale for these objects.

Galaxy Name		Hubble	D_{25}	Pixel scale	R_{CR}		R_{bar}		$\mathcal{R}_{PD} = \frac{R_{CR}}{R_{bar}}$	$\mathcal{R}_{CM} = \frac{R_{CR}}{R_{bar}}$	% differ
PGC	NGC	Type	(")	("'/pix)	(pix)	(")	(pix)	(")	PD method	Computer modeling	
02182	0165	SB(rs)bc	92.9	0.33	25.45±3.49	8.52±1.17	20.98±1.00	7.02±0.33	1.21±0.18	—	—
02388	0201	SAB(r)c	109.2	0.36	31.70±2.32	11.38±0.83	19.36±1.00	6.95±0.36	1.64±0.15	—	—
03377	0309	SAB(r)c	181.2	0.45	14.46±2.13	6.47±0.95	9.00±1.00	4.03±0.45	1.61±0.30	—	—
04367	0428	SAB(s)m	244.4	0.51	32.83±1.36	16.72±0.69	29.70±1.00	15.13±0.51	1.11±0.06	—	—
07210	—	SB(r)c	79.1	0.31	19.53±1.13	6.09±0.35	14.44±1.00	4.51±0.31	1.35±0.12	—	—
10122	1042	SAB(rs)cd	280.6	0.54	10.11±2.98	5.47±1.61	5.52±1.00	2.99±0.54	1.83±0.63	—	—
10496	1087	SAB(rs)c	222.9	0.49	18.89±0.36	9.24±0.18	18.49±1.00	9.05±0.49	1.02±0.06	—	—
12655	—	SABcd	58.6	0.27	13.61±1.46	3.73±0.40	14.44±1.00	3.96±0.27	0.94±0.12	—	—
13421	—	SAB(r)cd	82.8	0.32	18.29±0.49	5.82±0.16	16.00±1.00	5.09±0.32	1.14±0.08	—	—
21119	—	SAB(s)c	62.8	0.28	18.85±1.88	5.32±0.53	17.22±1.00	4.86±0.28	1.09±0.13	—	—
21291	—	SBcd	77.3	0.31	20.92±0.95	6.46±0.29	13.99±1.00	4.32±0.31	1.50±0.13	—	—
21513	—	SB(s)d	65.8	0.29	26.49±0.66	7.63±0.19	16.40±1.00	4.72±0.29	1.62±0.11	—	—
21978	—	SBdm	60.0	0.28	14.47±0.49	4.00±0.14	8.41±1.00	2.33±0.28	1.72±0.21	—	—
22205	—	SB(r)b	97.3	0.34	36.19±1.75	12.36±0.60	29.16±1.00	9.96±0.34	1.24±0.07	—	—
22453	2503	SAB(rs)bc	62.8	0.28	35.97±0.74	10.15±0.21	30.25±1.00	8.54±0.28	1.19±0.05	—	—
23047	—	SAB(rs)bc	97.3	0.34	23.46±0.51	8.01±0.17	20.25±1.00	6.91±0.34	1.16±0.06	—	—
23170	—	SBcd	80.9	0.32	21.69±1.01	6.83±0.32	16.40±1.00	5.17±0.32	1.32±0.10	—	—
23504	—	SB(s)cd	92.9	0.33	10.70±1.15	3.58±0.38	9.00±1.00	3.01±0.33	1.19±0.18	—	—
24641	—	SBb	68.9	0.29	16.61±0.69	4.88±0.20	10.89±1.00	3.20±0.29	1.53±0.15	—	—
26445	2840	SB(rs)bc	62.8	0.28	30.74±6.18	8.68±1.74	13.69±1.00	3.86±0.28	2.25±0.48	—	—
26982	—	SAB(rs)bc	51.1	0.26	33.38±3.78	8.62±0.98	30.80±1.00	7.95±0.26	1.08±0.13	—	—
27777	2964	SAB(r)bc	173.0	0.44	26.39±0.53	11.57±0.23	27.04±1.00	11.85±0.44	0.98±0.04	—	—
29539	—	SABb	80.9	0.32	21.60±4.28	6.81±1.35	19.80±1.00	6.24±0.32	1.09±0.22	—	—
29671	—	SAB(rs)c	95.1	0.34	11.98±0.81	4.05±0.27	11.56±1.00	3.91±0.34	1.04±0.11	—	—
31236	—	SBbc	65.8	0.29	17.09±0.43	4.92±0.12	14.82±1.00	4.27±0.29	1.15±0.08	—	—
32266	3374	SBc	75.5	0.31	23.84±1.12	7.29±0.34	24.50±1.00	7.49±0.31	0.97±0.06	—	—
32680	—	SB(s)b	68.9	0.29	26.73±2.91	7.86±0.86	22.56±1.00	6.63±0.29	1.18±0.14	—	—
32729	—	SBcd	53.5	0.26	34.37±1.06	9.05±0.28	19.36±1.00	5.10±0.26	1.78±0.11	—	—
33140	3485	SB(r)b	137.5	0.40	34.56±4.70	13.71±1.86	27.56±1.00	10.93±0.40	1.25±0.18	—	—
33240	—	SAB(r)bc	—	—	18.50±0.73	—	18.49±1.00	—	0.98±0.07	—	—
33325	—	SAB(r)c	72.1	0.30	21.08±1.51	6.32±0.45	13.69±1.00	4.10±0.30	1.54±0.16	—	—
33689	—	SAB(r)bc	75.5	0.31	22.02±0.54	6.73±0.17	20.52±1.00	6.27±0.31	1.07±0.06	—	—
34018	—	SBcd	58.6	0.27	25.02±0.67	6.85±0.18	18.92±1.00	5.18±0.27	1.32±0.08	—	—
34195	3577	SB(r)a	84.8	0.32	33.60±0.61	10.81±0.20	27.56±1.00	8.86±0.32	1.22±0.05	—	—
34232	3583	SB(s)b	169.1	0.43	27.65±3.55	12.00±1.54	23.52±1.00	10.21±0.43	1.18±0.16	1.24±0.23	5.08
35123	3668	SBbc	104.3	0.35	26.61±0.60	9.36±0.21	14.44±1.00	5.08±0.35	1.84±0.13	—	—
35458	—	SB(rs)b	—	—	28.51±1.433	—	16.81±1.00	—	1.70±0.13	—	—
35676	3726	SAB(r)c	370.0	0.61	22.54±1.29	13.75±0.79	18.49±1.00	11.28±0.61	1.22±0.10	1.95±0.55	59.84
35901	—	SB(s)b	—	—	16.44±1.79	—	13.32±1.00	—	1.23±0.16	—	—
36824	—	SAB(r)ab	101.9	0.35	27.91±6.38	9.72±2.22	20.25±1.00	7.05±0.35	1.38±0.32	—	—
37091	—	SBbc	80.9	0.32	15.06±0.34	4.75±0.11	11.56±1.00	3.64±0.32	1.30±0.12	—	—
38693	4145	SAB(rs)d	353.3	0.60	23.44±2.74	14.01±1.64	12.04±1.00	7.20±0.60	1.95±0.28	—	—
41101	4457	SAB(s)0/a	161.5	0.43	22.19±4.66	9.44±1.98	15.21±1.00	6.47±0.43	1.46±0.32	0.98±0.23	32.88
41934	4548	SB(rs)b	322.2	0.57	32.06±5.63	18.41±3.23	26.52±1.00	15.23±0.57	1.21±0.22	1.21±0.22	1.68
42168	4579	SAB(rs)b	353.3	0.60	43.51±4.03	26.01±2.41	23.04±1.00	13.77±0.60	1.89±0.19	1.46±0.30	22.75
42575	4618	SB(rs)m	250.1	0.51	31.65±0.59	16.28±0.30	25.00±1.00	12.86±0.51	1.27±0.06	—	—
42797	4643	SB(rs)0/a	185.4	0.45	44.24±5.68	19.98±2.57	40.96±1.00	18.50±0.45	1.08±0.14	1.04±0.19	3.70
42857	4654	SAB(rs)cd	293.9	0.55	19.67±0.25	10.85±0.14	16.40±1.00	9.05±0.55	1.20±0.07	—	—
42970	4665	SB(s)0/a	228.1	0.49	36.90±5.22	18.24±2.58	33.64±1.00	16.63±0.49	1.10±0.16	0.88±0.29	20.00
44032	—	SB(rs)bc	75.5	0.31	31.04±0.26	9.49±0.08	21.16±1.00	6.47±0.31	1.47±0.07	—	—
44797	4900	SB(rs)c	134.3	0.39	30.73±0.97	12.07±0.38	27.04±1.00	10.62±0.39	1.14±0.06	—	—
45015	4932	SAB(r)c	90.8	0.33	15.52±0.87	5.14±0.29	14.06±1.00	4.66±0.33	1.10±0.10	—	—
45781	—	SB(rs)c	79.1	0.31	27.27±3.22	8.51±1.00	23.33±1.00	7.28±0.31	1.17±0.15	—	—
48930	5305	SB(r)b	92.9	0.33	32.03±3.95	10.72±1.32	33.64±1.00	11.26±0.33	0.95±0.12	—	—

Table 2. Continued

Galaxy Name		Hubble	D_{25}	Pixel scale	R_{CR}		R_{bar}		$\mathcal{R}_{\text{PD}} = \frac{R_{\text{CR}}}{R_{\text{bar}}}$	$\mathcal{R}_{\text{CM}} = \frac{R_{\text{CR}}}{R_{\text{bar}}}$	% differer
PGC	NGC	Type	($''$)	($''/\text{pix}$)	(pix)	($''$)	(pix)	($''$)	PD method	Computer modeling	
52365	5701	SB(rs)0/a	255.9	0.52	33.23±1.88	17.27±0.98	23.04±1.00	11.97±0.52	1.44±0.10	1.44±0.10	41.48%
53979	5850	SB(r)b	255.9	0.52	44.73±4.27	23.24±2.22	36.00±1.00	18.71±0.52	1.24±0.12	1.39±0.29	12.10%
54849	5921	SB(r)bc	293.9	0.55	25.60±5.17	14.13±2.85	22.09±1.00	12.19±0.55	1.16±0.24	1.25±0.23	7.76%

tion closer to the bar ends) are most likely due to the bar pattern speed.

Uncertainty in radius is created when we are unable to distinguish if a phase crossing actually occurs in the light from the galaxy or if it is a result of the uncertainty in the values of the phase angle at that radius. Because the image data is divided into 2° wide azimuthal sections, and the output is assigned to the midpoint of the section, each phase angle could conceivably be within $\pm 1^\circ$ of the reported value. For our sample galaxies, we located the first phase crossing after the end of the bar, then identified the area around that crossing where the difference in the phase angle in the g and z wavebands was greater than 2° . The nearest smaller radius with $|\theta_g - \theta_z| > 2^\circ$ is the minimum corotation radius, $R_{\text{CR},\text{min}}$, and the next larger radius with $|\theta_g - \theta_z| > 2^\circ$ is the maximum corotation radius, $R_{\text{CR},\text{max}}$.

Occasionally plots of phase angle versus radius will have two phase crossings very close to each other. In these cases the corotation radius may actually be a region or range. In Aguerri et al. (1998) they defined “close together” as $< 5''$ apart. When listing a corotation value, they used the midpoint of the two phase crossings. A similar approach was taken here. If two or more phase crossings occurred between $R_{\text{CR},\text{min}}$ and $R_{\text{CR},\text{max}}$, then the average of the crossings is listed as the corotation radius.

The PD method was applied successfully to 57 galaxies from the EFIGI catalogue, although a total of 100 galaxies were inspected visually. 43 galaxies were excluded for the following reasons:

- There were problems with the galaxy images:
 - For 7 galaxies, IRAF could not determine the center of the galaxy for at least three wavebands.
 - For 10 galaxies, there was significant contamination from a large foreground object.
 - For 1 galaxy there was a significant satellite trail through one of the images.
 - For 4 galaxies, the bar and/or arms could not be identified due to a high degree of flocculency.
 - For 1 galaxy, the bar was much longer than any of the other galaxies in our sample.
- There were problems with the galaxy analysis:
 - The phase angle data was too erratic/noisy for 18 galaxies.
 - The range of $R_{\text{CR},\text{min}}$ to $R_{\text{CR},\text{max}}$ was too great for 1 galaxy.
 - There was trouble determining the end of the bar for 1 galaxy.

2.7 Calculation of the Relative Bar Pattern Speed

As mentioned in Section 1, “fast” bars may be indicative of low dark matter concentrations. For this reason, the relative bar pattern speed, \mathcal{R} , was calculated for each galaxy by dividing the corotation radius (R_{CR}) determined in section 3 by the bar radius (R_{bar}) determined in section 2.4. If $\mathcal{R} = R_{\text{CR}}/R_{\text{bar}} \geq 1.4$, the bar is defined as a “slow” rotator. If $\mathcal{R} < 1.4$, the bar is a “fast” rotator (Debattista & Sellwood 2000). In fact, even if the relative pattern speed, \mathcal{R} , isn’t necessarily related to the dark halo (see, e.g., Athanassoula 2013), it is still a good way to standardize comparisons of pattern speeds between galaxies. Note: In the cases where the error in the relative bar pattern speed, \mathcal{R} , is consistent with both a “fast” and “slow” speed, we classify the bar as “intermediate”.

3 RESULTS AND DISCUSSION

The results of the application of the PD method for finding the bar CR radius and the subsequent calculation of the relative bar pattern speed for the 57 galaxies are stated in Table 2. Shown in the table are the PGC name, the NGC name (if available), the D_{25} from de Vaucouleurs et al. (1991; RC3) and the calculated pixel scale (in $''/\text{pixel}$) for each galaxy. Table 2 also includes the bar corotation radius (R_{CR}) and bar radius (R_{bar}) in pixels and arcseconds. The relative bar pattern speed that we have calculated (\mathcal{R}_{PD}) is given, along with that determined from Sticky Particle simulations (\mathcal{R}_{CM}) by Rautiainen et al. (2008), and the percentage difference between them. Finally, Table 2 also lists the bar pattern speed as determined from the potential-density phase-shift method (BZ09).

Figure 2 shows the range of relative bar pattern speeds found for the 57 galaxies in our sample. The fastest bars are marked in black on the left of the figure. There are 34 galaxies that are classified as fast, $\mathcal{R} \leq 1.4$, even within the error bars. The 9 slowest bars are marked in black on the right of the figure. These galaxies are classified as slow because their bar pattern speeds, $\mathcal{R} > 1.4$, even within the error bars. The remaining 14 galaxies are in the middle of the figure. They are marked grey and have been termed intermediate because including the uncertainty in the bar pattern speed means that they are consistent with both slow and fast rotating bars. Of these 14 galaxies, 6 have a calculated $\mathcal{R} \leq 1.4$, and 8 have a calculated $R > 1.4$.

The 57 galaxies all had at least one major phase crossing, indicating the bar CR radius, that occurred near the end of the bar or further out in the galaxy. A subset of 15 of those galaxies had at least two major phase crossings. These galaxies are listed in Table 3 along with the radial position

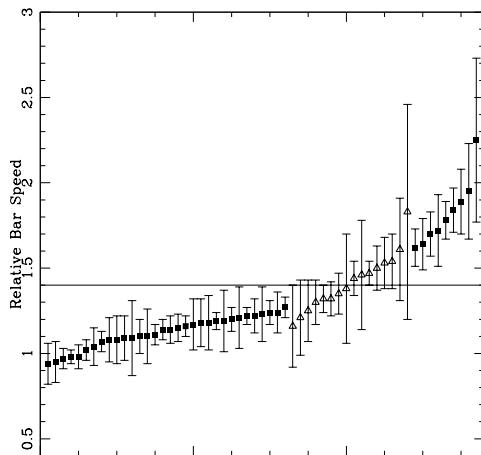


Figure 2. Range of relative bar pattern speeds for the 57 galaxies in roughly increasing order. The fastest bars are represented by solid squares on the left side. The slowest bars are also in solid squares on the right side. The hollow triangles in the middle represent galaxies with intermediate bars, where the relative bar speeds are consistent with both fast and slow patterns. The horizontal line corresponds to $\mathcal{R} = 1.4$, which is the divide between fast and slow bars (Debattista & Sellwood 2000).

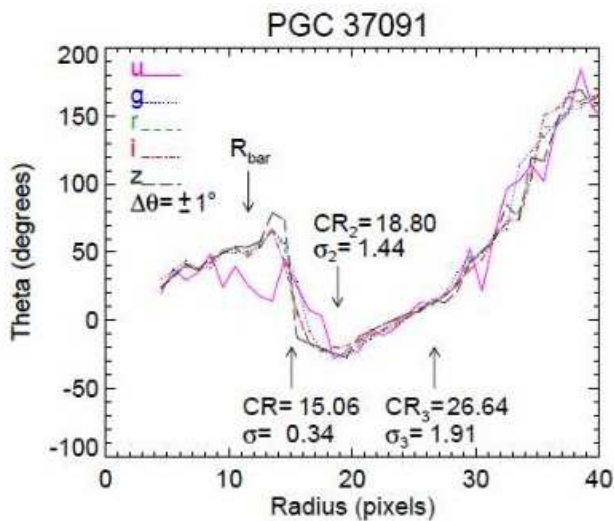


Figure 3. Plot of phase shift versus radius for PGC 37091. Three major phase crossings are shown.

(in pixels and arcsec) of the first and second phase crossings. The relative bar pattern speed for the first crossing \mathcal{R} and the relative bar pattern for second phase crossing \mathcal{R}_2 are both presented. It is possible that the second phase crossing corresponds to the transition zone (see Cepa & Beckman 1990). It is also possible the second phase crossing corresponds to the CR of the bar pattern speed, while the first crossing corresponds to a nuclear bar pattern speed. If the second crossing goes with the major bar, then the relative bar pattern speed is listed in the last column named \mathcal{R}_2 .

Aguerri et al. (1998) suggested that crossings within $5''$ of each other could be considered a corotation range. Table 3

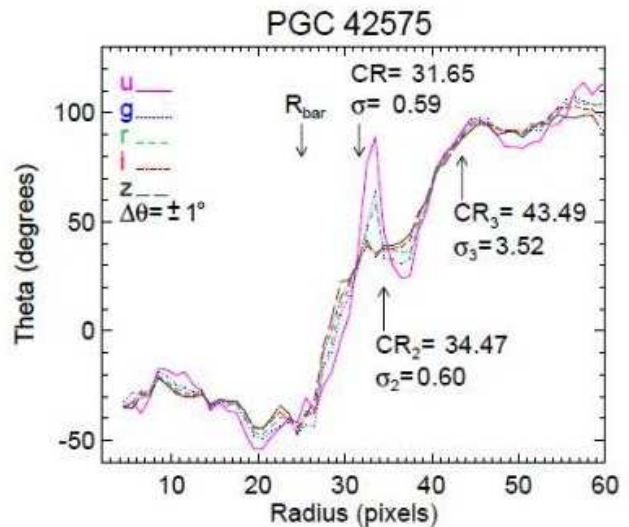


Figure 4. Plot of phase shift versus radius for PGC 42575. Three major phase crossings are shown.

therefore also lists the difference between the two CR radii. The bold values are greater than $5''$ when the uncertainties are considered. The non-bold values correspond to galaxies with a possible bar corotation region instead of a specific bar corotation radius. Please note that the separation of $< 5''$ between adjacent phase crossings to identify a corotation range, as suggested by Aguerri et al. (1998), may be somewhat simplistic. For example, the separation between the phase crossings for PGC 21119 is $R_{CR2} - R_{CR} = 4.53$, indicating that it may have a corotation range. However, the pattern speed for the bar in this range varies from $\mathcal{R} = 1.09 \pm 0.13$ to $\mathcal{R}_2 = 2.03 \pm 0.13$. With such a large difference in the relative bar pattern speed, it is difficult to imagine this as a corotation range, but rather two distant CR radii. We therefore caution the reader, not only to consider the difference between CR radii, but also the range of determined bar pattern speeds. Alternatively, a physical separation (measured in kpc) may be a more useful parameter, than an angular separation.

Two of the 57 galaxies had 3 major phase crossings. All three crossings are shown in Figures 3 and 4. The third phase crossing might correspond to the spiral arm pattern speed (Cepa & Beckman 1990, their Figure 1). The pixel scale (in $''/\text{pixel}$) for PGC 37091 is 0.32. The difference between CR2 and CR is $R_{CR2} - R_{CR} = 3.74$ pixels or $1.20''$ and the difference between CR3 and CR is $R_{CR3} - R_{CR} = 3.71''$. The pixel scale for PGC 42575 is 0.51. The difference between CR2 and CR is $R_{CR2} - R_{CR} = 2.82$ pixels or $1.44''$. However CR3 is separated from CR by $R_{CR3} - R_{CR} = 6.04''$.

3.1 Comparing PD with Sticky Particle modeling

For sticky-particle simulations a near-infrared image is used to derive a gravitational potential of the galaxy. Then “sticky” particles, i.e., particles that lose energy in collisions, are used to model the response of the cold gas component of the galaxy to the underlying gravitational potential. The dynamical parameters of the computer simulation are varied until the simulated galaxy’s morphology, such as rings and

Table 3. Data for the 15 galaxies with more than one CR radius. Columns 1 and 2 list the galaxy name as given in the PGC and NGC catalogues respectively; Columns 3 and 4 list the first (inner) corotation radius in pixels and arcseconds respectively; Columns 5 and 6 list the second (outer) corotation radius in pixels and arcseconds respectively; Column 7 gives the difference between the outer and inner corotation radii in arcseconds; Column 8 gives the relative bar pattern speed for the inner corotation radius; and Column 9 gives the relative bar pattern speed for the outer corotation radius.

Galaxy Name		R_{CR}		R_{CR2}		$R_{CR2} - R_{CR}$	$\mathcal{R} = R_{CR}/R_{bar}$	$\mathcal{R}_2 = R_{CR2}/R_{bar}$
PGC	NGC	(pixels)	(arcsec)	(pixels)	(arcsec)	(arcsec)		
03377	0309	14.46±2.13	6.47±0.95	19.28±1.17	8.62±0.52	2.16	1.61±0.30	2.14±0.27
10122	1042	10.11±2.98	5.47±1.61	19.45±3.02	10.52±1.63	5.05	1.83±0.63	3.52±0.84
10496	1087	18.89±0.36	9.24±0.18	39.05±1.62	19.11±0.79	9.87	1.02±0.06	2.11±0.14
12655	—	13.61±1.46	3.73±0.40	21.30±1.21	5.83±0.33	2.11	0.94±0.12	1.48±0.13
13421	—	18.29±0.49	5.82±0.16	38.07±0.97	12.12±0.31	6.30	1.14±0.08	2.38±0.16
21119	—	18.85±1.88	5.32±0.53	34.89±0.95	9.85±0.27	4.53	1.09±0.13	2.03±0.13
21291	—	20.92±0.95	6.46±0.29	31.52±1.59	9.74±0.49	3.27	1.50±0.13	2.25±0.20
21978	—	14.47±0.49	4.00±0.14	33.36±0.72	9.23±0.20	5.23	1.72±0.21	3.97±0.48
23047	—	23.46±0.51	8.01±0.17	32.68±1.00	11.16±0.34	3.15	1.16±0.06	1.61±0.09
24641	—	16.61±0.69	4.88±0.20	27.58±0.49	8.11±0.14	3.22	1.53±0.25	2.53±0.24
37091	—	15.06±0.34	4.75±0.11	18.80±1.44	5.92±0.45	1.18	1.30±0.12	1.63±0.19
41934	4548	32.06±5.63	18.41±3.23	38.16±1.53	21.91±0.88	3.50	1.21±0.22	1.44±0.08
42575	4618	31.65±0.59	16.28±0.30	34.47±0.60	17.73±0.31	1.45	1.27±0.06	1.38±0.06
42857	4654	19.67±0.25	10.85±0.14	27.69±2.21	15.28±1.22	4.43	1.20±0.07	1.69±0.17
44797	4900	30.73±0.97	12.07±0.38	36.33±1.84	14.27±0.72	2.20	1.14±0.06	1.34±0.08

arm curvature, matches the real galaxy image (e.g., Rautiainen et al. 2008; Treuthardt et al. 2009, 2012).

The spiral arms are matched by comparing their location, pitch angle, and extent. Using this method the pattern speed that fits the outer parts of the galaxy might be different from the pattern speed for the fit for the inner parts. A possible explanation for this difference is that different galaxy morphological features may have different pattern speeds (i.e., a bar may have a different pattern speed when compared to spiral arms; see e.g., Sellwood & Sparke 1988). When Rautiainen et al. encountered multiple fits, they chose the lowest relative pattern speed to represent the bars pattern speed (Rautiainen et al. 2008).

To validate the PD method, a sample of barred spiral galaxies, with previously determined relative bar pattern speeds, \mathcal{R} , were chosen from the EFIGI dataset. The sample galaxies were selected because their \mathcal{R} were also determined using computer simulations in a study by Rautiainen et al. (2008). These authors used virtual particles to simulate the response of gas molecules in a gravitational potential for 38 barred spiral galaxies. Ten of these galaxies were included in the EFIGI dataset. We applied the PD method to the ten common galaxies and found the results to be consistent with the values reported by Rautiainen et al. (2008). The results for these 10 galaxies are shown in Figure 5.

As shown in Table 2, the relative bar pattern speed of 9 of the 10 sample galaxies studied using the PD method are consistent (within the 1- σ errors) with the results obtained by the computer simulations of Rautiainen et al. (2008). The galaxy without consistent results is PGC 35676 (NGC 3726). However the values for this galaxy with their uncertainties, $\mathcal{R}_{PD} = 1.22 \pm 0.10$ for the PD method and $\mathcal{R}_{CM} = 1.95 \pm 0.55$ using computer modeling, nearly overlap, and they definitely overlap within the 2- σ errors (the quoted errors are 1- σ), so one could argue that, even for NGC 3726, the bar pattern speed determined here, and that determined by Rautiainen et al. (2008), are consistent.

Note that in Table 2, we include the calculated pixel

scale (in "/pixel) and the R_{bar} and R_{CR} in both pixels and arcseconds. Since the relative bar pattern speed, \mathcal{R} , is a dimensionless parameter, the choice of units for R_{bar} and R_{CR} are not that important. We feel that this information is useful for readers who wish to use EFIGI data in the future.

Figure 5 shows a bar corotation radius for PGC 35676 at $R_{CR} = 22.54 \pm 1.29$ pixels, the first phase crossing after the end of the bar. If our identified bar length of $R_{bar} = 18.49 \pm 1.00$ pixels is multiplied by the relative bar pattern speed found using computer modeling, $\mathcal{R} = 1.95 \pm 0.55$, the corotation radius, $R_{CR} = \mathcal{R}_{CM} * R_{bar} = 36.05 \pm 10.35$ pixels. Visual inspection of PGC 35676 in Figure 5 shows another phase crossing at $\simeq 38$ pixels. It is possible the pattern speed reported by Rautiainen et al. (2008) refers to a different corotation or resonance location.

3.2 Comparing PD with the potential-density phase-shift method

The potential-density phase-shift method uses near-infrared images to infer the gravitational potential and density of a galaxy. The potential and density spirals are azimuthally shifted from each other. The locations where the phase shift changes, signals a corotation radius. For an S-shaped spiral or bar, the sign convention is to “assume the phase shift is positive when the potential lags the density pattern in the direction of galactic rotation” (Zhang & Buta 2007; hereafter ZB07).

In Buta & Zhang (2009; hereafter BZ09), the corotation radii were determined using the potential-density phase-shift method. Then, relative bar pattern speeds for 101 galaxies were calculated from their corotation radii, using the bar radii derived by Laurikainen et al. (2004). The results include “super-fast” bars, i.e., bars with $\mathcal{R} < 1$ (BZ09). This is controversial as a bar with a pattern speed $\mathcal{R} < 1$ should not be self-consistent, and therefore, should not be long-lived (Contopoulos 1980).

We were able to determine corotation radii and relative bar pattern speeds for 17 of the galaxies from the BZ09 sample (see Table 2). This includes all ten of the galaxies from Figure 5 that had measurements of \mathcal{R} and R_{CR} from the Rautiainen et al. (2008) study. Generally, the results using the PD method are inconsistent with the ZB07 method. However uncertainties were not included in the BZ09 results. It is possible that a calculation of those uncertainties would show the two methods to actually be consistent with each other. Additionally, because of the controversial “super-fast” bars derived from the method used by BZ09, their results are in conflict with the popular view of self-sustaining bars (Contopoulos 1980).

The relative bar pattern speeds from BZ09 are included in Table 2. Figure 6 shows results from the PD method for the 7 galaxies that were not included the Rautiainen et al. (2008) method.

3.3 Implications for Dark Matter Concentrations

Figure 7 shows the phase crossings and information for which CR radii could be determined using the PD method for the 40 remaining galaxies.

Within the quoted errors, all 57 of the galaxies in our sample have relative bar pattern speeds of $\mathcal{R} = 1.0$ or greater. This is consistent with the results of Contopoulos (1980), who find that the radius of a bar cannot be larger than its CR radius, or the bar would not be self sustaining (i.e., it would not exist).

As can be seen from the values of the relative bar pattern speed, \mathcal{R} , in both Table 2 and Figure 2, 34 out of 57 galaxies have “fast” bars with $\mathcal{R} \leq 1.4$. From the results of Debattista & Sellwood (2000), we would expect this to indicate that these galaxies have dark matter halos with a low Navarro, Frenk & White (1997) concentration parameter, c . This is due to reduced dynamical friction between the bar and the halo.

In seeming contradiction to this conclusion, Athanassoula (2014) showed via N -body+SPH simulation models that galaxies with submaximal disks have widely differing values of \mathcal{R} , ranging from fast to slow, when only slow bars are expected. From these results, she argues that \mathcal{R} does not indicate a constraint of the halo density.

Recently, Sellwood & Debattista (2014) have argued that Athanassoula’s simulations (2014) do in fact agree with the conclusion that maximum disks models have $\mathcal{R} \sim 1.2 \pm 0.2$. Her models with varied gas fractions, but similar mass distributions initially, should not all experience the same dynamical friction. Instead, the rearrangement of mass in the early evolution of a galaxy makes gas-rich disks more maximal. This leads to less dynamical friction between the forming bar and the halo, giving a lower measured value of \mathcal{R} .

The net result of these arguments allows us to conclude that low NFW concentrations exist in 34 out of 57 galaxies in our sample due to their fast bars.

4 CONCLUSIONS

We have applied the photometric PD method for determining CR radii and relative bar pattern speeds to a sample

of 57 galaxies. Of these galaxies, 17 had CR radii that had been determined via other methods in the literature. For these 17 galaxies, we obtain results that are generally consistent with those found using the sticky-particle simulation method (Rautiainen et al. 2008). Our results appear to be inconsistent with the more controversial phase density method used by BZ09. It should be noted that the phase density method is controversial, primarily because BZ09 have used it to determine that some bars are “super-fast”, and (as explained above), this should not be possible (Contopoulos 1980). Unfortunately, we were unable to find any galaxies in the EFIGI catalogue for which the bar pattern speed had been determined using the TW method. The TW method is generally considered the best approach for determining bar speeds, since it is the only method which measures bar speed directly. Nevertheless, there is an indication that sticky-article modeling and TW measurements produce similar results within the errors (Treuthardt et al. 2009). Our comparison of the PD method with the sticky-particle simulation (Rautiainen et al. 2008) method shows very promising results.

Using the dynamical results of Debattista & Sellwood (2000), we argue that most of the galaxies in our sample (34 out of 57) have “fast” bars. This would indicate a low NFW concentration.

Finally, our results have implications on models that explain the nature of spiral structure in disk galaxies. Generally, resonances (including the CR) are expected from any type of spiral density wave (e.g., Lin & Shu 1964; Bertin et al. 1989a, b; Bertin 1993; Bertin & Lin 1996), or even swing amplification (e.g., Toomre 1981; Fuchs 2001). However, the color gradients we find across spiral arms appear inconsistent with the predictions of manifold theory (Romero-Gomez et al. 2006, 2007; Athanassoula et al. 2009a, b, 2010; Athanassoula 2012). In manifold theory, particles (i.e., gas or stars) flow along the manifold (the spiral arm), rather than across it. It is the flow of gas across a density wave that leads to the color changes we see across spiral arms. The color gradients we find in our sample of 57 galaxies, suggest that manifold theory is not in operation in these objects.

It should be noted that the sample of 57 galaxies that we have studied here was drawn from a parent sample of 100 galaxies. In the parent sample, we found phase profiles for 18 galaxies that were erratic or noisy. As there was no clear phase crossing for these 18 objects, this could be evidence that supports manifold theory in these particular galaxies. We therefore suggest that, while density wave theories explain spiral structure in most disk galaxies, there are some that may be better explained with manifold theory. However, it is clear that larger datasets need to be studied in order to come to any solid conclusions.

ACKNOWLEDGMENTS

The authors wish to thank the Arkansas Space Grant Consortium for their support and funding, without which the results presented here would not have been possible. We also thank Thomas Mears for his assistance in defining the sample of galaxies that was used in this paper. IP acknowledges the Mexican Foundation Conacyt for financial support. The

authors wish to thank the anonymous referee whose comments improved the content of this paper.

REFERENCES

- Adelman-McCarthy J. K., Agüeros M. A., Allam S. S., et al., 2006, *ApJS*, 162, 38
- Aguerri J. A. L., Beckman J. E., Prieto M., 1998, *AJ*, 116, 2136
- Athanassoula E., 2012, *MNRAS*, 426, L46
- Athanassoula E., 2014, *MNRAS*, 438, L81
- Athanassoula E., Romero-Gómez M., Masdemont J. J., 2009a, *MNRAS*, 394, 67
- Athanassoula E., Romero-Gómez M., Bosma A., Masdemont J. J., 2009b, *MNRAS*, 400, 1706
- Athanassoula E., Romero-Gómez M., Bosma A., Masdemont J. J., 2010, *MNRAS*, 407, 1433
- Baillard A., Bertin E., de Lapparent V., et al., 2011, *A&A*, 532, A74 (EFIGI)
- Beckman J. E., Cepa J., 1990, *A&A*, 229, 37
- Bertin E., Arnouts S., 1996, *A&AS*, 117, 393
- Bertin G., 1993, *PASP*, 105, 640
- Bertin G., Lin C. C., 1996, *Spiral Structure in Disk Galaxies*, MIT press: Cambridge
- Bertin G., Lin C. C., Lowe S. A., Thurstans R. P., 1989a, *ApJ*, 338, 78
- Bertin G., Lin C. C., Lowe S. A., Thurstans R. P., 1989a, *ApJ*, 338, 104
- Binney J., Tremaine S., 2008, *Galactic Dynamics: Second Edition*, Princeton University Press: Princeton
- Buta R. J., Zhang X., 2009, *ApJS*, 182, 559 (BZ09)
- Contopoulos G., 1980, *A&A*, 81, 198
- de Vaucouleurs G., de Vaucouleurs A., Corwin H. G., Buta R. J., Paturel G., Fouqué P., 1991, *Third Reference Catalogue of Bright Galaxies*, Springer: New York (RC3)
- Debattista V. P., Sellwood J. A., 2000, *ApJ*, 543, 704
- Eskridge P. B., Frogel J. A., Rogge R. W., et al., 2000, *AJ*, 119, 536
- Fuchs B., 2001, *A&A*, 368, 107
- Hernandez O., Wozniak H., Carignan C., et al., 2005, *ApJ*, 632, 253
- Laurikainen E., Salo H., Buta R., Vasylyev S., 2004, *MNRAS*, 355, 1251
- Lin C. C., Shu F. H., 1964, *ApJ*, 140, 646
- Lin L.-H., Yuan C., Buta R., 2008, *ApJ*, 684, 1048
- Martínez-García E. E., Gonzalez-Lopezlira R. A., 2013, *ApJ*, 765, 105
- Martínez-García, E. E., Puerari I., 2014, *ApJ*, 790, 118
- Martínez-García E. E., González-Lópezlira R. A., Bruzual A. G., 2009a, *ApJ*, 694, 512
- Martínez-García E. E., González-Lópezlira R. A., Gómez G. C., 2009b, *ApJ*, 707, 1650
- Navarro J. F., Frenk C. S., White S. D. M., 1997, *ApJ*, 490, 493
- Patsis P. A., Skokos C., Athanassoula E., 2003, *MNRAS*, 346, 1031
- Paturel G., Fouqué P., Bottinelli L., Gouguenheim L., 1989, *A&AS*, 80, 299
- Puerari I., Dottori H., 1997, *ApJ*, 476, L73 (PD)
- Rautiainen P., Salo H., Laurikainen E., 2008, *MNRAS*, 388, 1803
- Roberts W. W., 1969, *ApJ*, 158, 123
- Romero-Gómez M., Masdemont J. J., Athanassoula E., Garcia-Gomez C., 2006, *A&A*, 453, 39
- Romero-Gómez M., Athanassoula E., Masdemont J. J., Garcia-Gomez C., 2007, *A&A*, 472, 63
- Salo H., Laurikainen E., Buta R., Knapen J. H., 2010, *ApJ*, 715, L56
- Seigar M. S., James P. A., 1998, *MNRAS*, 299, 672
- Seigar M. S., James P. A., 2002, *MNRAS*, 337, 1113
- Sellwood J. A., Debattista V. P., 2014, arXiv:1410.0834
- Sellwood J. A., Sparke L. S., 1988, 1988, 231, L25
- Toomre A., 1981, in *The Structure and Evolution of Normal Galaxies*, Ed. S. M. Fall & D. Lynden-Bell, Cambridge Univ. Press: New York, p. 111
- Tremaine S., Weinberg M. D., 1984, *ApJ*, 282, L5 (TW)
- Treuthardt P., Salo H., Buta R., 2009, *AJ*, 137, 19
- Treuthardt P., Seigar M. S., Sierra A. D., et al., 2012, *MNRAS*, 423, 3118
- Wozniak H., Friedli D., Martinet L., et al., 1995, *A&AS*, 111, 115
- Zhang X., Buta R., 2007, *AJ*, 133, 2584 (ZB07)

This paper has been typeset from a \TeX / \LaTeX file prepared by the author.